Boundary-Condition Analysis of an Idealized Left Atrium Model

Dueñas-Pamplona, J., Sierra-Pallares, J., García, J. et al..

Published 05 January 2021

Boundary-Condition Analysis of an Idealized Left Atrium Model

JORGE DUENAS-PAMPLONA,[1] JOSE´ SIERRA-PALLARES,[2]
JAVIER GARCIÁ,[1] FRANCISCO CASTRO,[2] and JORGE MUNOZ-PANIAGUA[1]

[1]Departamento de Ingeniería Energética, Escuela Técnica Superior de Ingenieros Industriales, Universidad Politécnica de Madrid, C/ José Gutiérrez Abascal 2, 28006 Madrid, Spain; and [2]Departamento de Ingeniería Energética y Fluidomecánica, Escuela de Ingenierías Industriales, Universidad de Valladolid, Paseo del Cauce 59, 47011 Valladolid, Spain

Abstract—The most common type of cardiac arrhythmia is atrial fibrillation (AF), which is characterised by irregular and ineffective atrial contraction. This behaviour results into the formation of thrombi, mainly in the left atrial appendage (LAA), responsible for thromboembolic events. Very different approaches are considered as therapy for AF patients. Therefore, it is necessary to yield insight into the flow physics of thrombi formation to determine which is the most appropriate strategy in each case. Computational Fluid Dynamics (CFD) has proven successful in getting a better understanding of the thrombosis phenomenon, but it still requires validation by means of accurate flow field *in vivo* atrial measurements. As an alternative, in this paper it is proposed an *in vitro* flow validation, consisting in an idealised model that captures the main flow features observed in the human LA which, once combined with Particle Image Velocimetry (PIV) measurements, provides readily accessible, easy to emulate, detailed velocity fields. These results have been used to validate our laminar and Large Eddy Simulation (LES) simulations. Besides, we have run a parametric study of different boundary conditions sets previously employed in the literature. These data can be used as a benchmark for further development of LA CFD models.

Keywords—Left atrial appendage, Atrial fibrillation, Model validation, Computational fluid dynamics, Particle image velocimetry, Ostium flow, Large eddy simulation.

INTRODUCTION

Cardiovascular diseases are globally the first mortality cause nowadays. Meanwhile, the most common type of cardiac arrhythmia is atrial fibrillation (AF), affecting 1 to 2% of the population, and about 8% of individuals over 80 years old.[17] In Europe and the USA, one in every four adults is believed to suffer AF at some point in his life.[25]

AF is characterized by irregular and ineffective atrial contraction, usually triggered by electrical impulses coming from the roots of the pulmonary veins (PV) in the left atrium (LA). It is also known to be related to thrombus formation episodes, carrying an increased all-cause mortality risk of two times in women and 1, 5 times in men and being as well the leading cause of thromboembolic events such as stroke and vascular dementia.[5]

Between 70 and 90% of left atrial thrombi responsible for thromboembolic AF-related events are originated in the left atrial appendage (LAA).[5,18] LAA is a 2–4 cm long, protruding and trabeculated cavity of the LA, characterized by a largely variable morphology from one patient to another in parameters such as size, height, smoothness and numbers of lobes. LAA acts in normal sinus rhythm as a contractile reservoir or as a decompression chamber, depending on the cardiac cycle phase. However, in AF conditions its contractility is drastically reduced, resulting in flow stagnation which is known to promote stasis and thrombus formation.

The therapy usually prescribed on AF patients older than 65 years old is oral anticoagulation (OAC), which helps to reduce the risk of thrombus formation.[18] But in case the OAC therapy is not appropriate, because of

the high risk of bleeding or other patient's limitations, LAA surgical exclusion or LAA percutaneous occlusion can be applied. Although it exists a range of commercial occlusion devices (WATCHMANr and AMPLATZERr are the most commonly used),[9] undeniably these options present some drawbacks and limitations,[1,18] such as vascular injury, air-embolic events and peri-device leaks. Other possibilities like rhythm and frequency cardiac control can improve the AF-related symptoms, but there is no evidence of their ability to reduce long-term mortality.

Consequently, in order to be able to identify patient groups and select the optimum therapy (either a therapeutic treatment or a surgical procedure), it is crucial to find a proper criterion to predict the thrombus formation risk.[26] Many different parameters have been used for this risk quantification: volume of the appendage, length of the appendage, number of lobes, ostium dimensions or velocities and the appendage shape (indicating the *chicken wing* morphology as the least critical and the *cauliflower* as the most).[14] Anyway, the existing studies have not come to an agreement and the criteria to quantify coagulation risk remains unclear.[22]

The usefulness of computational fluid dynamics (CFD) to assist cardiac diagnosis has been strongly proved by several works.[4,29] In this sense, some CFD studies have presented numerical analyses of the flow patterns in the LA,[11,19,24] with some of them including the LAA in the model and considering AF conditions.[6,16,23] But even though these previous studies have been able to provide important insights into the AF phenomenon, and also to calculate otherwise inaccessible parameters related to thrombus formation such as residence times, vorticities and shear stresses, their common weakness seems to be the difficulty to select accurate boundary conditions and validate the numerical model.

That may be due in part to the difficulty to obtain *in-vivo* information about the velocity fields accurate enough to validate numerical models. Pulmonary veins (PV) or mitral valve (MV) measured doppler-velocities have been sometimes used to compare with numerical results but, as projected point-wise velocities, they cannot provide an accurate flow validation. Although Phase Contrast Magnetic Resonance Imaging (PC-MRI or 4D-Flow techniques) is giving encouraging prospects regarding this issue,[15,19] nowadays it is not fully developed to assess numerical simulation reliability in the left atrium. Thus, there is a lot of uncertainty about the reliability of numerical codes simulating physiological conditions, which question the findings obtained through numerical simulation.

To overcome this problem, in this research we perform an *in-vitro* flow validation in an experimental set-up which reproduces the most important atrial flow characteristics, such as the high transient nature of the flow and its vortex formation patterns.[27] To the best of our knowledge, this study pioneers in the development of a benchmark for computational haemodynamics of this kind. To this end, an idealized model of the LA has been designed in order to perform velocity field measurements in a reproducible and well-controlled experimental set-up using the Particle Image Velocimetry (PIV) as flow measurement technique. This experimental set-up avoids the particularities of patient-specific geometries and allows to obtain a rich set of experimental data for benchmarking fluid dynamic models of the LA.

This paper will first discuss the experimental setup and the simulation model in ''Materials and Methods'' section, presenting the design of the idealized model, the measuring process and the details of the simulation model. Then in ''Results'' section, the results of flow velocities and patterns are presented. Finally, the results are discussed in ''Discussion'' section, where also the limitations and conclusions of the study are drawn.

MATERIALS AND METHODS

This section includes the description of the experimental setup and the numerical model.

Experimental Setup

Since the objective of the experimental results is to provide highly controlled measurements of a simplified flow for numerical validation, obtaining a stable and controlled cyclic flow rate was a priority over respecting full dynamic similarity with blood flow. The set-up has been designed to replicate somehow the complex flow structure that takes place in the LA and LAA, including high-transient flows, vortex formation and emptying and filling appendage flow patterns.

The idealized model, Fig. 1, is made of Poly Methyl Methacrylate (PMMA), and is composed by two main parts: the LA body (115.2 mL) and the LAA body (21.4 mL), which are connected together by the elliptical ostium (251.2 mm^2). Four circular section inlets (78 mm^2 each one) role the play of the pulmonary veins (PV). As the flow pattern in LA is highly influenced by the orientation of the PV, these conduits are located by pairs, replicating the geometric usual arrangement of the PV: inflow from the right pulmonary veins (RPV) follows the smooth contour of the atrial wall towards the MV, whereas the inflow from the left pulmonary veins (LPV) turns abruptly after entry to head towards the MV. It has been observed in 4-D Flow Magnetic Resonance Imaging (4-D Flow MRI) studies[15] that

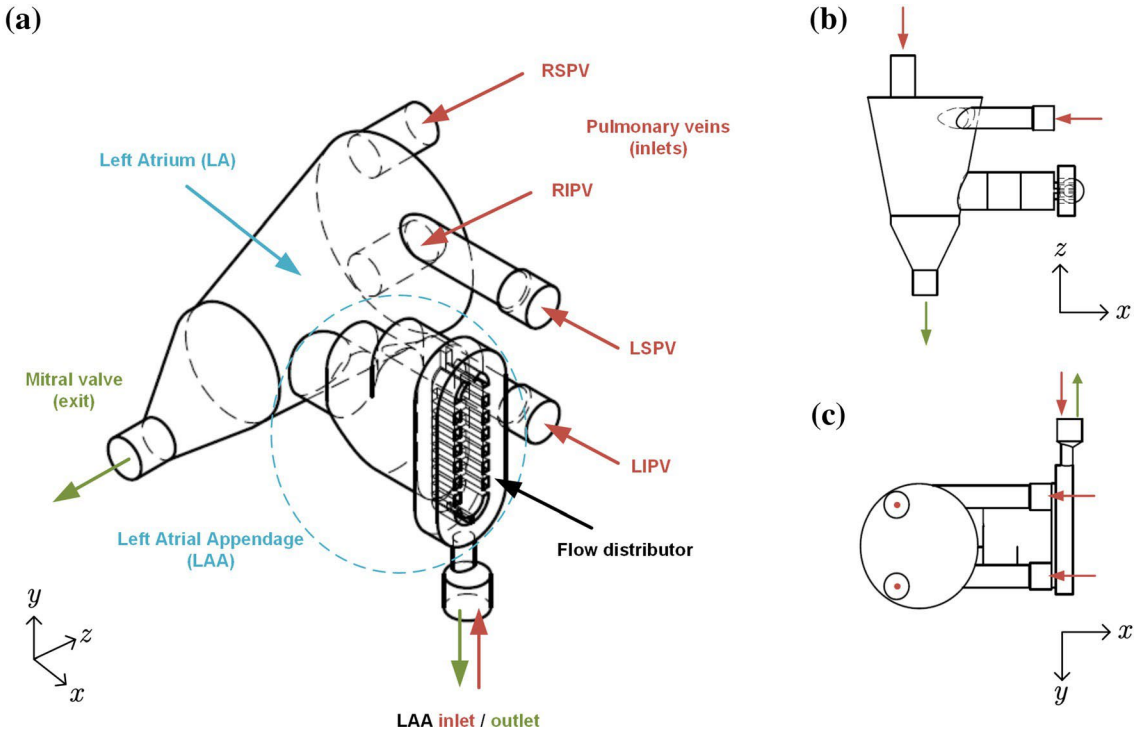

FIGURE 1. Diagram indicating the main parts of the left atrial idealized model, showing different views: (a) perspective view, (b) top view and (c) front view. The incoming flows are marked in red and the outgoing flows are marked in green.

this results in the formation of two transient vortex when the atrial flow is decelerated during the cardiac cycle, one during the systole and the other in the late diastole. That vortex is initiated mainly by the LPV flow, while the RPV flow is confined between the vortex and the atrial walls. The main outlet which plays the role of the MV in the idealized model is disposed at the end of the LA body, with an area of 450 mm^2. Regarding the LAA geometry, it has been designed with three protruding lobes. In Table 1 the baseline and the typical physiological values[3,11–13,16,20] are given.

TABLE 1. Baseline characteristics.

	Model	Physiological
Cycle length (s)	1.0	0.6–1.0
Systole (s)	0.4	0.3–0.4
Diastole (s)	0.6	0.3–0.7
LA volume (mL)	115.2	36.1–146
LAA volume (mL)	21.4	5–40
MV area (mm^2)	850.2	572.5–962.1
PV area (mm^2)	105.2	78.5–283.5
Ostium area (mm^2)	251.2	176.7–490.9

In the physiological LAA, the cavity filling begins during the ventricular systole, when both the LA and the LAA increase their volume because of the PV incoming flow.[27] During the early diastole and the LV relaxation, the LAA is partially emptied. After that, and coincident with atrial systole, the LAA contracts itself contributing to increase the MV flow. Therefore, the LAA flow can be described as a two-stage flow induced by its walls deformation, both passively and actively.

To be able to replicate this two-stage LAA flow behaviour, a flow has been allowed to exit and enter the model in a controlled way through a distributor placed at the end of the LAA body, as can be seen in Fig. 1. In this way, we were able to replicate the natural expansion and contraction of the LAA during the cardiac cycle found in Doppler transesophageal echocardiography.[2] Adjusting this flow through the ostium, three different cases have been designed:

- Type I. ''Healthy case'' (flexible LAA): Patient in sinus rhythm with a regular LAA pattern of filling and emptying, keeping a lower incidence of thromboembolism. The two-stage LAA flow has been achieved by setting an incoming flow during diastole and an outgoing flow during systole.
- Type II. ''AF case'' (semi-rigid LAA): Patient with reduced LAA contractility, ejection fraction, and inflow and outflow velocities, which is associated with risk of thrombus formation. To reproduce the

typical AF ''sawtooth'' pattern, a compliance has been installed at the end of the appendage. A plastic tube of 120 mm of length, 8 mm of diameter and 750 N=mm^2 of elastic modulus has been selected for this purpose.

- Type III. ''Extreme AF case'' (rigid LAA): Patient with drastically reduced LAA contractility, ejection fraction, and inflow and outflow velocities, which is associated with a high risk of sudden thrombus formation. To reproduce the absence of identifiable flow waves, the diffuser at the end of the model has been completely closed, not letting the flow to pass through.

A schematic diagram of the experimental facility is shown in Fig. 2. Flow is originated by the difference in height between a constant level reservoir and the discharge level. The fluid was a mixture of 39 wt% distilled water and 61 wt% glycerin to emulate blood behaviour.[7] The refracting index of the fluid matches that of the model material (PMMA), ensuring to avoid optical distortion. Density and viscosity are 1151 kg=m^3 and 0.007 pa s, respectively. The fluid enters the circuit from the constant level reservoir, being directed by the four PVs to the LA model.

To reproduce the systole and diastole parts of the cardiac cycle, three solenoid-valves are used. These valves provided a highly stable and controlled cycle. During the diastole the valves E1 and E2 are open and E3 closed, directing the flow towards the MV. When there is no flow through MV during the systole, fluid entering the pulmonary veins is directed and recirculated in the LAA (E1 and E2 closed and E3 open). The maximum flow is adjusted by needle valves. A pump returns the liquid discharged in the lower reservoir to the constant level reservoir.

In physiological conditions, during diastole, blood leaves the LA through the open MV with a first strong ejection and second weaker one. During systole MV closes, and the LA is filled with blood coming from pulmonary veins enlarging it and LAA.[6,13,15] The experimental cycles last 1 s (600 ms diastole and 400 ms systole, respectively). The Womerseley number is $\alpha \approx 10$, indicating that the flow will be dominated by transient effects.[21] The temporal evolution of the flow is shown in Fig. 4, for each one of the three cases previously mentioned. They are different because of the disparity in the LA and LAA contractilities,.[11] The flow is positive when enters in the LA. Although the measured

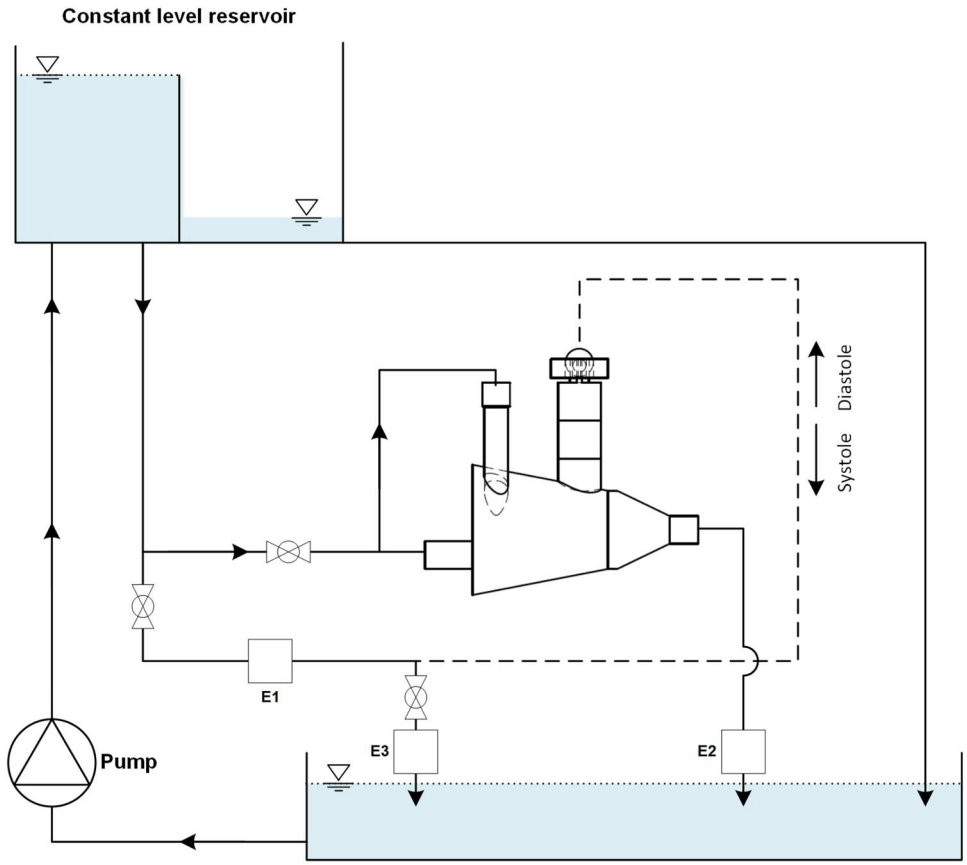

FIGURE 2. Diagram of the experimental facility showing up the main parts: idealized LA model, the control valves E1, E2 and E3, the pump and the reservoirs.

flow is not strictly physiological due to physical limitations associated with the experimental setup, it successfully reproduces many atrial flow characteristics such as rapid changes in ostium flow direction, making it possible to perform the validation of the numerical model for high-transient flow.

A Dantec 2D2C PIV system composed of an Nd:YAG Dantec Dynamics Dual-Power 200-15 laser and a CCD Dantec Dynamics FlowSense 4M MkII camera, with a 2048 × 2048 pixels resolution, positioned perpendicularly to the laser sheet was used at the measurements. The fluid was seeded with 15 μm fluorescent polymeric particles. Measurements were performed at different selected instants through various consecutive cycles. An averaging procedure is carried out for each measurement to obtain mean values of velocity components at the selected instants. Regarding data processing, the Interrogation Area (IA) was set to 32 × 32 pixels (0.87 × 0.87 mm^2) in all cases, with a 0% overlap. The time delay between pulses was set in order to obtain maximum particle image displacement within the IA of 25% of the side length.[28] One hundred pairs of images were found to be enough to make the velocity vector map independent from the number of images and reach statistical convergence. The recorded image pairs were analyzed by a Fourier based two-frame cross-correlation algorithm (Dantec DynamicStudio v3.14). Next, an ensemble velocity field average is obtained.

For the fields of view considered, uncertainty in the scale factor under study was less than 0.8 %; uncertainty in the time between images is set by the PIV system (0.3%). Finally, uncertainty in the particle image displacement calculation was estimated based on the cross-correlation peak ratio proposed by Charonko *et al.*[10] for standard cross-correlation. An example of an uncertainty field can be found in Fig. 3, where it can be observed an uncertainty around 8 % in most of the distribution. There are small shadows in the surroundings of images taken. As a consequence, velocity calculated in this affected IA yielded a less precise result. This effect can be appreciated in Fig. 3, where these regions can easily be recognized by their increase in the velocity uncertainty values. For the final uncertainty estimation, 8 % is used since it is the most common value. The measurements were performed at a 25 ± 1 ºC fluid temperature. The uncertainty in Re number because of viscosity is estimated as less than 8.4 %.

Numerical Setup

The simulation was performed using the commercial software ANSYSr Fluent 2019R3 (ANSYS, Inc. Products). There are still doubts on whether the atrial flow is entirely laminar, so we have decided to perform both the laminar and LES models, since LES is very adequate in these cases where a transitional flow can appear. Both advection and transient schemes were second-order accurate, and a convergence criteria of 10^{-4} was used. The ''Coupled'' scheme was selected as pressure-velocity coupling algorithm for the laminar model, while bounded central differencing for momentum equations and the ''SIMPLE'' method for pressure-velocity coupling was selected for the LES model.

The fluid was assumed to have the same density ρ and dynamic viscosity μ as in the experimental setup: 1151 kg/m^3 and 0.007 pa s respectively. The effect of non-Newtonian behavior of blood is not significant and it is thus considered to be negligible. The flow has been computed by solving the continuity and Navier–Stokes equations (Eqs. 1 and 2 respectively) where v is the velocity vector and p is the pressure,

$$\nabla \cdot v = 0 \qquad (1)$$

$$\frac{\partial v}{\partial t} + v \cdot \nabla v = -\frac{\nabla p}{\rho} + \frac{\mu}{\rho}\nabla^2 v \qquad (2)$$

The walls of the model have been considered to be rigid, replicating the appendage contraction by imposing the measured inflow and outflow through the diffuser at the end of the LAA shown in Fig. 1. A Savitzky–Golay filter has been employed to obtain smoother profiles from the experiments suitable for CFD: original profiles are represented by a thin line in Fig. 4, while the filtered ones are represented by a thicker line.

To study the effect of different types of boundary conditions in MV and PV, 5 different cases have been implemented and compared:

- Case 1 is generated by setting the same velocity profile for each of the four PV, and a constant pressure level in the MV. These boundary conditions have been employed in previous works by Garcia-Isla *et al.*[16] and Aguado *et al.*[1] The imposed velocity profile has been obtained experimentally by performing an equal distribution of the flow measured with PIV between each of the four PV.
- Case 2 is obtained by setting a zero constant pressure in the pulmonary veins and a velocity profile calculated from the measured flow at the MV outlet. In this way, different flowrates are allowed to enter the computational domain *via* each PV. This boundary condition set has been employed in the works of Bosi *et al.*[6]

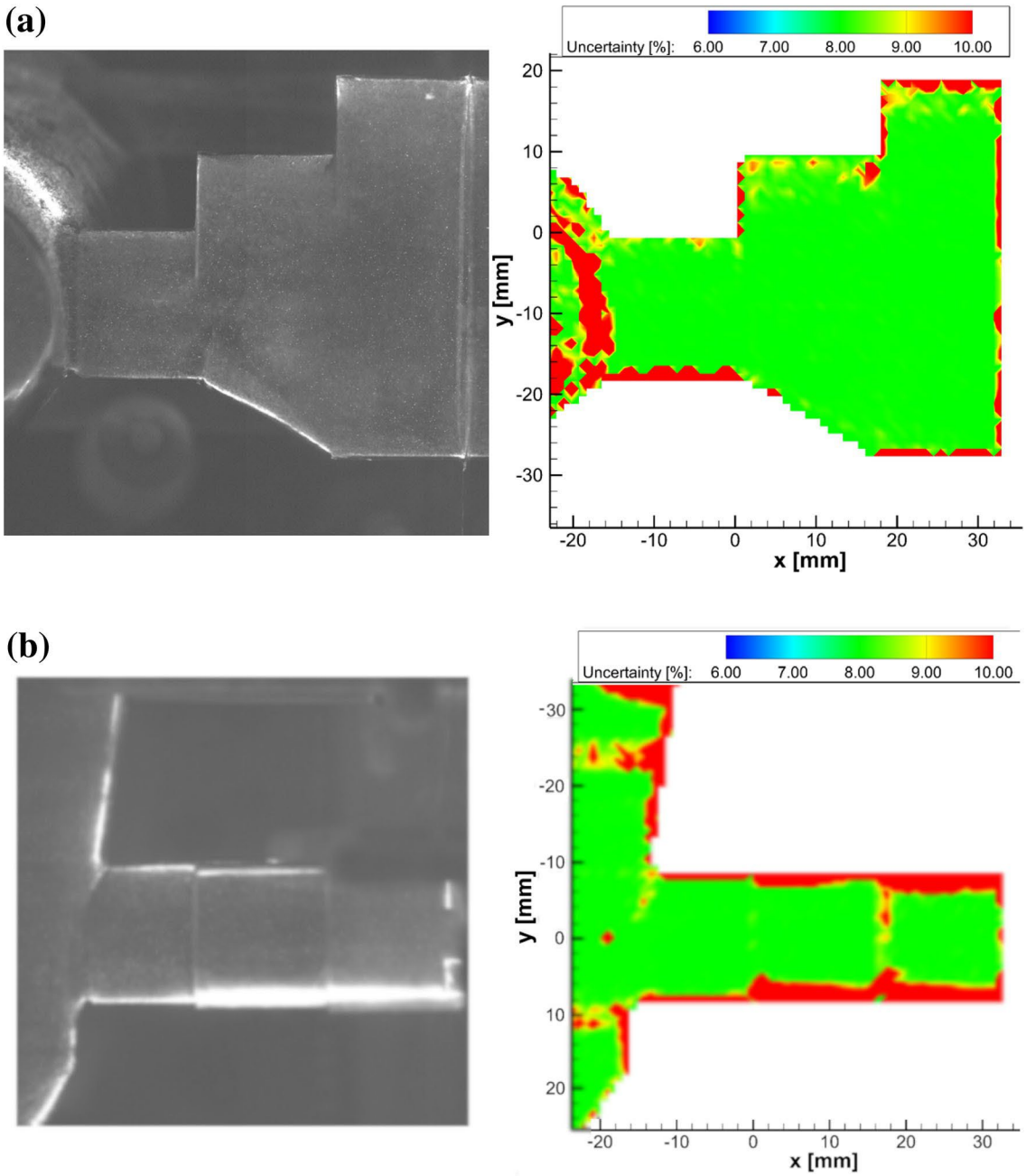

FIGURE 3. Example of PIV uncertainty fields for the model in two views: (a) LAA xy plane and (b) LAA xz plane.

- Case 3 is generated by setting the same velocity profile for each of the four PV, and a velocity profile in the MV calculated from the measured flow.
- Case 4 takes advantage of the measured MV pressure profile, imposing it in combination with the measured PV velocity profile.
- Case 5 is the opposite to Case 4; measured PV pressure profile and measured MV velocity profile have been imposed.

Case 4 and Case 5 are not common in the computational haemodynamics literature, as it is not easy to obtain a patient-specific flow and pressure profiles at the same time. This range of different boundary conditions sets allows for the study of different cases, comparing their convergence behaviour and the accuracy of their predictions. In Table 2 a summary of the boundary conditions employed can be found.

The MV was considered to be closed during ventricular systole and opened during the ventricular diastole, being the opening and closing time ’ 10 ms.

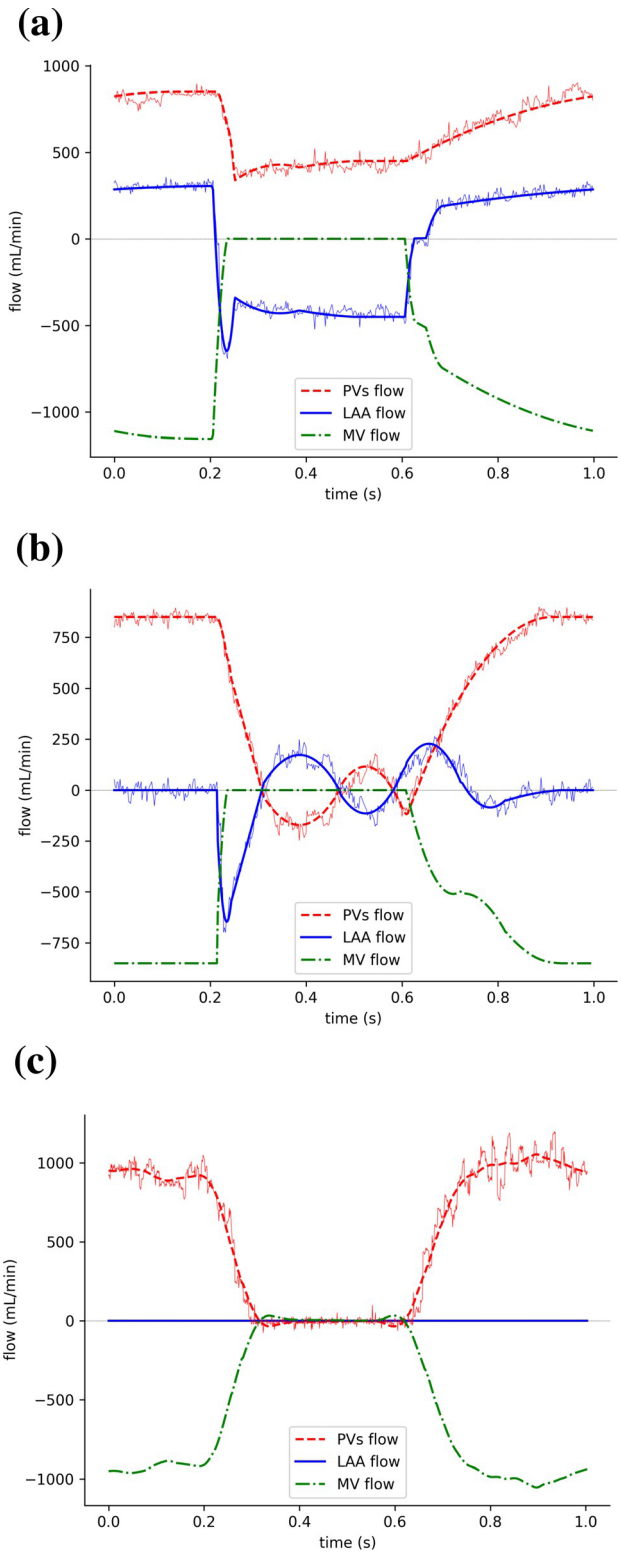

FIGURE 4. Flow profiles measured for the different LAA conditions: (a) healthy case, (b) AF case and (c) extreme AF case.

TABLE 2. Summary of the different boundary condition sets employed in the model.

LAA behaviour	
Type I—Synus rhythm	LAA: Sinus rhythm
Type II—AF case	LAA: "Sawtooth pattern"
Type III—Extreme AF case	LAA: Rigid
Boundary conditions sets	
Case 1	PV: Flow profile MV: Constant pressure
Case 2	PV: Constant pressure MV: Flow profile
Case 3	PV: Flow profile MV: Flow profile
Case 4	PV: Flow profile MV: Pressure profile
Case 5	PV: Pressure profile MV: Flow profile

The blood flow analysis has been conducted with a time increment of $1\mathrm{O}^{-3}$ s, changing it to $5 \times 1\mathrm{O}^{-4}$ s in the most transient parts of the cycle to adjust the Courant number.

Tetrahedral volumetric meshes have been generated using ANSYSr Meshing^{TM}(ANSYS, Inc. Products), being the computational domain bounded by the inlets and outlets of the experimental model (previously shown in Fig. 1). A mesh convergence study was conducted to confirm that the mesh did not substantially influence the solutions, being the velocity differences between the selected mesh and a more refined one less than 4% of velocity relative error. Two meshes have been finally selected, being the number of cells 587,622 and 1,270,000 for the laminar and LES model respectively.

A time convergence analysis has been performed. It has been shown that the simulation loses memory of the initial conditions from the fifth cycle on. Thus, the results are based on the sixth cycle of each simulation. The velocity field relative temporal error is less than 2% between cycles in the selected planes.

Evaluation of the simulation framework was performed by quantitative comparison between the simulated flow patterns and the experimental ones. Flow patterns were assessed by both velocity magnitudes and vectors at two cross-sectional planes: the LAA *xy* plane and the LAA *xz* plane, whose definitions are shown on Fig. 5 in blue and green respectively.

RESULTS

In this section the validation of the numerical model and the boundary condition analysis are presented. It has been achieved by comparing the simulated velocity

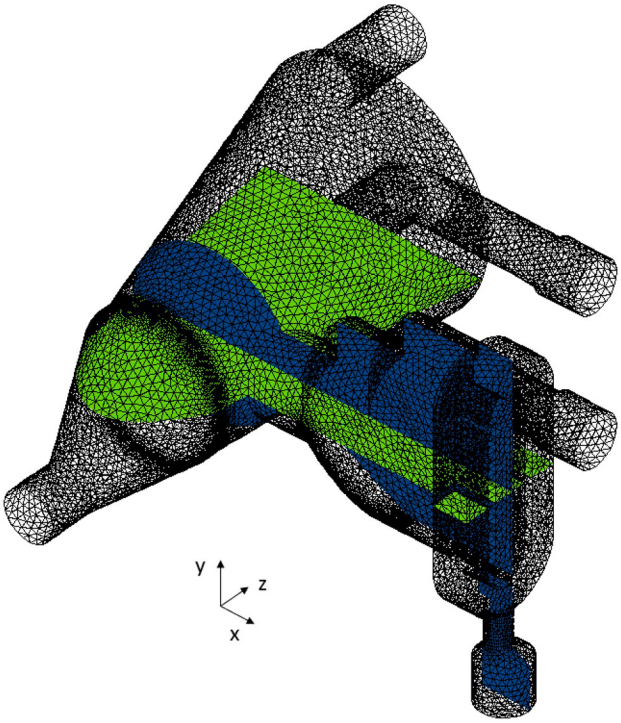

FIGURE 5. Computational mesh and reporting planes: LAA xy plane is displayed in blue and LAA xz plane in green.

fields and flow patterns with the experimental PIV measurements.

As stated in the previous section, three different LAA behaviours have been experimentally described: a ''Healthy case'' with a normal filling and emptying pattern, an ''AF case'' with a reduced LAA contractility and an ''Extreme AF case'' with the LAA totally rigid. For each one of this different cases, five numerical experiments have been performed. Each different numerical experiment represents one of the boundary condition sets shown in Table 2.

The experimental and simulated v_{xy} and v_{xz} vector fields have been then interpolated into a sufficiently dense 2D mesh (being v_{xy} and v_{xz} the projections of the velocity in the selected planes xy and xz), allowing to perform a quantitative vector field comparison point by point. Two magnitudes have been chosen to compare the velocity fields: the probability distribution function (PDF) of the relative error $\mathrm{d}|v_{xy}|$ normalized with half the maximum velocity, and the PDF of the angular misalignment h between the measured and the simulated vector. These angular misalignment values should range from 0° when the velocity fields are completely aligned to 180° when there exists a total lack of alignment. The formal definitions of the relative error $\mathrm{d}|v_{xy}|$ and the angular misalignment h can be found in Eqs. (3) and (4) respectively,

$$\mathrm{d}|v_{xy}| = \frac{|v_{xy}^{\mathrm{PIV}}| - |v_{xy}^{\mathrm{CFD}}|}{\frac{1}{2}|v_{xy}^{\mathrm{MAX}}|}\,100\%] \qquad (3)$$

$$\mathrm{h} = \arccos\left(\frac{v_{xy}^{\mathrm{PIV}} \cdot v_{xy}^{\mathrm{CFD}}}{|v_{xy}^{\mathrm{PIV}}|\,|v_{xy}^{\mathrm{CFD}}|}\right)\frac{180}{\pi}\,^{\circ}] \qquad (4)$$

Figures 6a and 6b show the velocity-magnitude contour comparison over time for LES and PIV results in the LAA xy plane, which successfully captured the filling and emptying of the LAA. For each measured contour, the relative error PDFs are shown in Fig. 6c for both the laminar and LES model. This error shows a very reasonable agreement with the experimental measurements, although not a perfect match.

Figures 7a and 7b show the same velocity-magnitude contour comparison over time between experimental and simulated velocity fields but in the LA xz plane. As in the previous one, for each measured contour, laminar and LES relative error PDFs are shown in 7c. In the bottom part the whole cycle is shown, with the selected cycle instants marked in red.

The global error and angle misalignment of the whole cycle have also been calculated, and its PDF is shown in Fig. 8. Here an average of all the cycle instants has been done. This allows to compare the grade of accuracy achieved with each one of the five different cases, and discriminating with the LAA behaviour (healthy, AF or extreme AF).

DISCUSSION

The strength of this study lies in the fact that it describes a series of highly controlled, experimental measurements for their application to atrial or LAA flow CFD model validation.

The designed set-up successfully describes the most relevant flow pattern in the LA: high transient nature of the flow and vortex formation due to the orientation of the pulmonary veins. Although the geometry is not physiological, it constitutes a well-designed test for a numerical code since it mimics the main challenges observed in a physiological situation. The rigidity of the material employed was compensated with the use of a diffuser at the end of the LAA: imposing a certain flow profile, installing a selected compliance or closing it totally has allowed the set-up to generate a range of different LAA contractility situations. The experimental model mimics the LA characteristics of an AF patient with a severe ventricular dysfunction, which is related with a dangerously high risk of thrombosis.[8]

In Fig. 6 the comparison between the velocity fields is shown for different time steps in the cycle for the ''Healthy case'', which reproduces a regular LAA

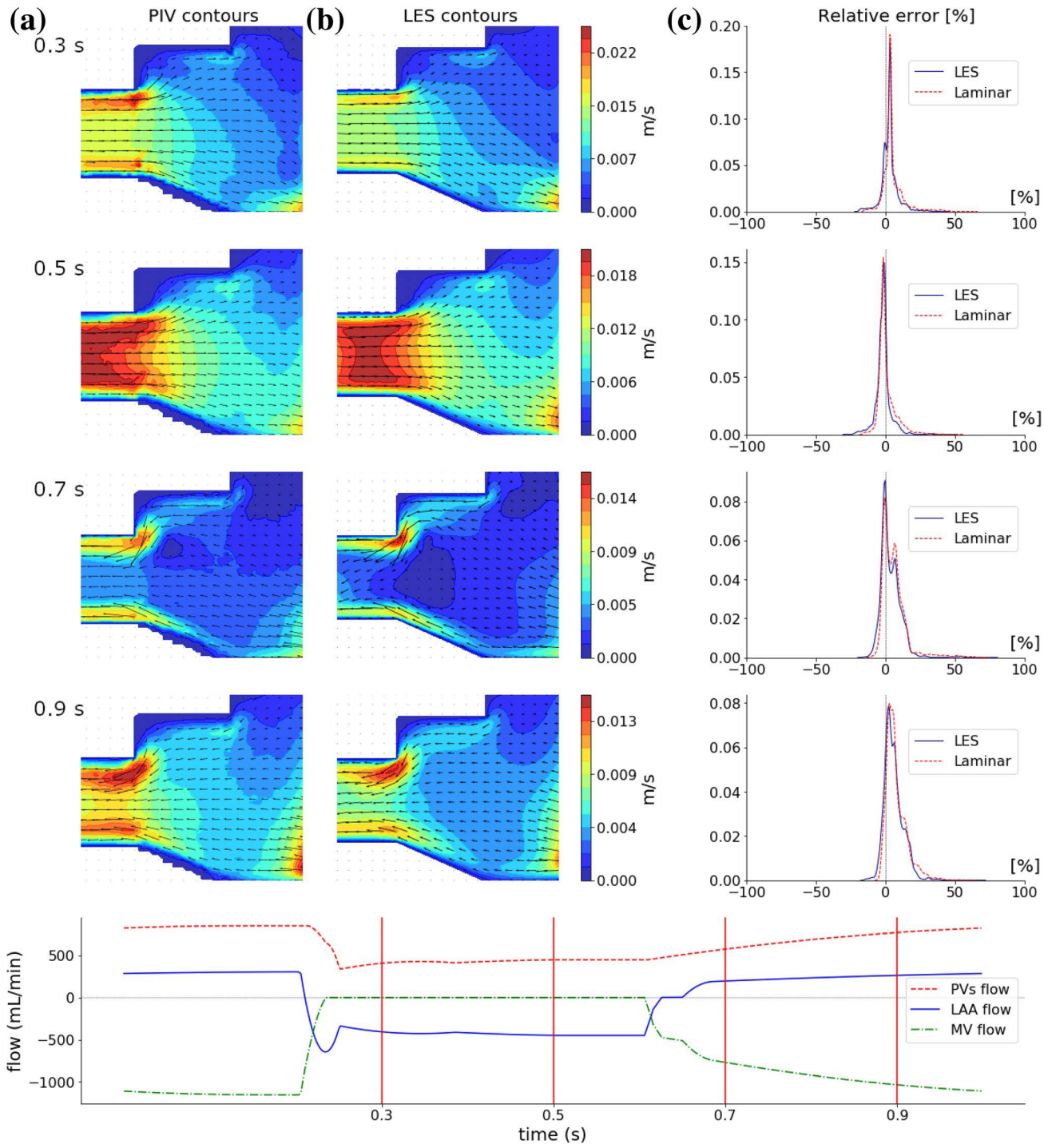

FIGURE 6. PIV-CFD ''Healthy case'' comparison between the experimental and simulated velocity contours. (a) PIV velocity contours in the xy plane for the instants 0.3, 0.5, 0.7 and 0.9 s. (b) LES velocity contours in the xy plane for the same cycle instants. (c) PDF Relative error between measured and simulated velocity contours, comparing laminar and LES simulations. At the bottom of the image the whole cycle is displayed.

pattern of filling and emptying, keeping a lower incidence of thromboembolism. The two-stage flow has been achieved by setting in the diffuser of the LAA model an incoming flow during systole and an outgoing flow during diastole. The first column displays the experimental velocity contours measured in the LAA *xy* plane, while the second one displays the simulated velocity field in this same plane. In the third and last column the PDF of the relative error is shown both for the laminar and LES model, calculated as a percentage

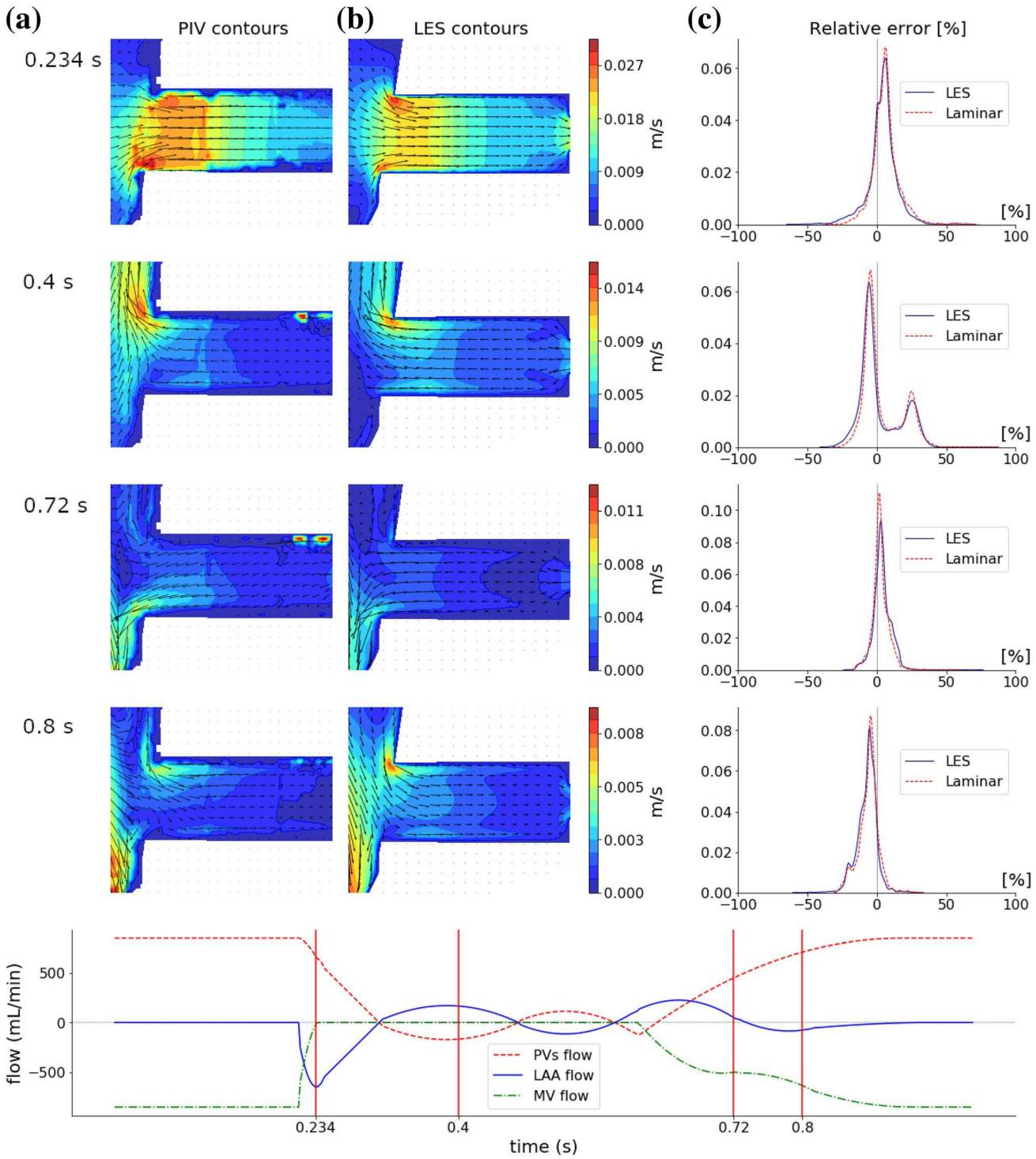

FIGURE 7. PIV-CFD ''AF case'' comparison between the experimental and simulated velocity contours. (a) PIV velocity contours in the xz plane for the instants 0.23, 0.4, 0.72 and 0.8 s. (b) LES velocity contours in the xz plane for the same cycle instants. (c) PDF Relative error between measured and simulated velocity contours, comparing laminar and LES simulations. At the bottom of the image the whole cycle is displayed.

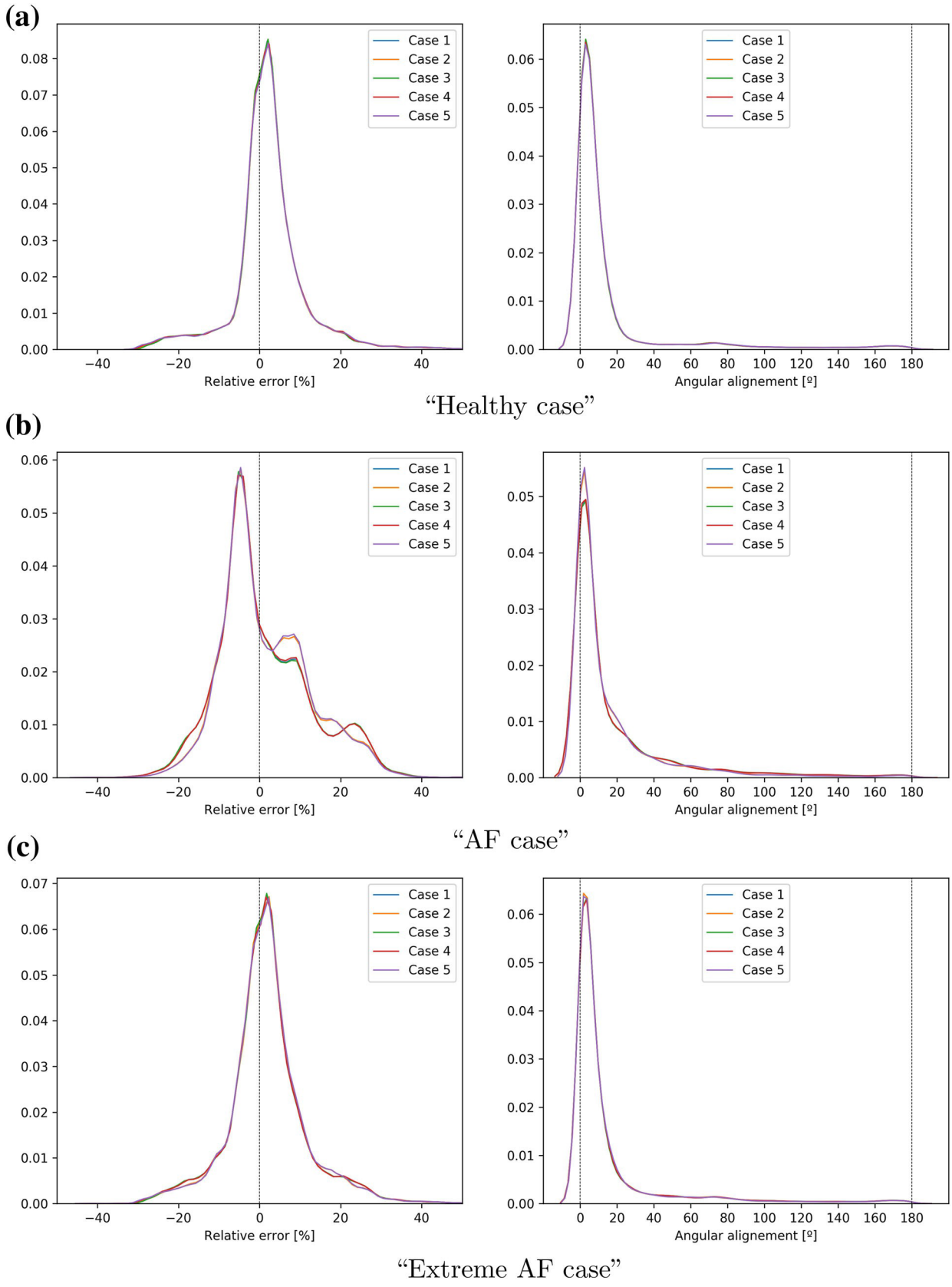

FIGURE 8. Boundary condition sets global error comparison. Laminar model.

of half the maximum velocity for each time step. At the bottom of the Fig. 6 the cycle flows can be seen, with the displayed time steps marked in red.

Four frames of the cycle are displayed in Fig. 6: 0.3, 0.5, 0.7 and 0.9 s. The first two instants (0.3 and 0.5 s) correspond to the systole part of the cycle, with the MV closed and pulmonary inflow causing the filling of the LAA. The last instants (0.7 and 0.9 s) correspond to the diastole, with the atrial flow passing through the MV. The LAA contributes to this ventricle filling flow, as proven by the outflow coming from the LAA. It can be seen that the flow through the LAA is not entirely symmetrical, which may be due to physical limitations in he performance of the diffuser and the geometry of the LAA which conditions the incoming flow.

The flow pattern in the ideal model has been successfully described: as in a real LAA case, the filling began during the ventricular systole, reaching its peak at the end of the reservoir phase. After that and during the diastole, it is emptied progressively. Here the highest ostium velocities are found during the LAA filling, which takes place during the systole. The velocity reaches its peak at the end of the reservoir phase. During the diastole the LAA contraction is mimicked by the outflow through the diffuser.

In Fig. 6c the good agreement reached between experimental and numerical results is shown, being the higher relative error located in the most critical measurement areas as expected (shadowed regions in Fig. 3). Little difference can be appreciated between laminar and LES model, which is consistent with the usual hypothesis of laminar flow in the left atrium.

It should be stressed how, when the flow accelerates to pass through the ostium, the higher velocities are obtained in the proximities of the ostium walls (see for example instant 0.7 s in Fig. 6). These are also the locations where the flow first changes its direction; this unsteady nature of fluid flow in response to an unsteady pressure gradient due to the pulsatile nature of the flow is sometimes described by the Womersley number.[21] This effect may lead to a wall shear stress increase near the ostium walls, being a factor that may lead to thrombus formation within the LAA or in the proximities of the ostium.

In Fig. 7 we can see ''AF case'', which reproduces typical AF ''sawtooth'' pattern.[2] This irregular LAA flow pattern has been successfully reproduced by installing an appropriate compliance at the end of the appendage. In this way it has been replicated the case of an atrium with reduced LAA contractility, ejection fraction, and inflow and outflow velocities, associated with risk of thrombus formation.

Four frames of the cycle are displayed in Fig. 7: 0.234, 0.4, 0.72 and 0.8 s. The first instant corresponds to the change between diastole and systole, while the MV is closing: this causes the flow coming from the PV to enter into the LAA. The instant 0.4 s pertains to the systole part of the cycle, with the MV closed. Here the pressure fluctuations present in the LA make the LAA to experiment successive expansions and contractions, generating an oscillatory flow through the ostium. The last instants (0.72 and 0.8 s) correspond to the diastole, with the LAA oscillatory flow being slowly attenuated. It can be seen that during the diastole the LAA does not contribute to the ventricle filling flow, due to its lack of contraction.

The flow pattern in the LAA during AF episodes has been successfully described: all the contraction and expansion that suffers the LAA is supposed to be passive, and due to atrial pressure changes. Here the highest ostium velocities are found at the beginning of the reservoir phase, which takes place during the systole (as can be seen in Fig. 4b). At the end of the diastole the ostium oscillatory flow is totally attenuated. This configuration shows also how the loss of contractility leads to the presence of reversal venous flow (Fig. 7).

The level of LAA contractility can vary, being the ''AF extreme case'' the worst case, where the LAA has lost every contractility and remains totally rigid (Fig. 4c). Here the total absence of identifiable flow waves leads to flow stagnation in the LAA, which is associated with an increased risk of sudden thrombus formation.

In Fig. 7c the relative error between experimental and numerical results can be seen. Although in this ''AF case'' the results are not as good as in the ''Healthy case'', as a reasonable agreement is achieved almost all over the LAA, the model can be considered as validated. Nevertheless, the discrepancy in this case lead us to be cautious with the accuracy of numerical models applied in physiological geometries with complex boundary conditions. It draws attention to the need of validation: it cannot be presumed the accuracy of any numerical model which has not been carefully validated.

In Fig. 8 the PDF of the global error and angle misalignment comparison of the different cases and numerical experiments are shown. The left part of the Fig. 8 shows the cycle global error $\mathrm{d}|v_{xy}|$ whereas the right part shows the global misalignment angle θ. Each row of Fig. 8 compares the results of a LAA flow case (Fig. 8a: ''Healthy case'', Fig. 8b: ''AF case'' and Fig. 8c: ''Extreme AF case''), being the labels of each sub-figure the numerical cases representing different boundary condition sets (Case 1–5, described in Table 2). As can be seen in Fig. 8, a high level of agreement has been achieved between the different numerical experiments. This indicates that every one of

them has converged to the same solution, being the differences between them practically negligible.

Case 1 is generated by imposing an equal distribution of the flow in each one of the PV, and a constant pressure level equal to zero in the MV (previously employed by Aguado *et al.*[1] and Garcia-Isla *et al.*[16]) This numerical experiment has been compared in Figs. 6 and 7, achieving a reasonable level of accuracy with measured flow fields in both cases. Case 2 is obtained inverting the boundary conditions present in Case 1: setting the zero constant pressure in the PV and imposing the measured flow in the MV. In this way, the existence of a different inflow from each PV is allowed. However, this existing difference between the PV flow distribution does not seem to affect the LAA flow: the differences observed between the ostium flows in both cases are negligible (the flow comparison in LAA *xy* plane can be seen in Fig. 8a). So it can be induced that the flow in the LAA is scarcely affected by the PV flow distribution or the boundary condition set in the MV; it would be more influenced by the PV orientations and the contractility of the LAA. Case 3 obtains the same results of Case 1 imposing the flow in both inlets and outlet. Cases 4 and 5 implement measured pressure profiles (in MV and PV respectively), leading to a slower convergence to finally reach the same flow solution. From these last two cases it can be concluded that disposing of pressure information in the PV and MV does not necessarily conduce to a better prediction of the flow in the LAA if accurate velocity distributions or any flow data is available.

CONCLUSIONS

A series of highly controlled, experimental measurements for their application to atrial flow CFD model validation has been performed. These measurements have been employed to tackle an *in-vitro* flow validation in a simplified atrium model, which to the best of our knowledge has not been done before. We have compared the laminar and LES models to verify the laminar hypothesis: no turbulent or transitional local flows have been detected, so the atrial flow can be considered as laminar. Working with this *in-vitro* model has not only allowed us to confirm the LAA flow patterns observed in previous studies, but also to extract general conclusions avoiding the particularities of patient-specific geometries. At the same time, the existence of a carefully validated model has allowed to check and compare in Figs. 6, 7 and 8 the accuracy of different sets of boundary conditions which have been employed in previous works. The high-transitory nature of the atrial flow and its vortex formation patterns have been replicated, which has allowed to observe how the LAA loss of compliance due to AF influences in the flow through the ostium, and therefore in the process of thrombus formation within the LAA. At the same time it has been observed the importance of the influence of the Womersley number in the velocity near the ostium walls, which may be associated with endothelial damage near the ostium walls and thus related to the process of thrombus formation. It should also be stressed the little effect that the PV flow distribution and MV boundary condition seem to have on the LAA flow, which seem to be governed mostly by the LAA contractility, the atrial pressure and the PV disposition and orientation in the LA. Furthermore, the results obtained in this research represent readily accessible, easy to emulate, detailed velocity fields and geometry, which can be used as a benchmark for further development of LA CFD models. The difference observed in some zones between the measured and calculated flow velocities illustrates the importance of carrying further studies related with atrial flow models validation, in a field where it is not always simple to obtain *in-vivo* accurate flow measurements.

ACKNOWLEDGMENTS

This work was supported by *Ministerio de Ciencia, Innovacio´n y Universidades of Spain* under contract DPI 2017-83911-R and by *Junta de Castilla y Leo´n* under Project ''Proyecto de apoyo a GIR 2018'' with reference VA081G18. We want to show our gratitude to the *Programa Propio—Universidad Polite´cnica de Madrid*, specially to its predoctoral contract Grants. We would also thank Alberto Pozo Álvarez who collaborated in early versions of this work and the CeSViMa UPM project for its computational resources.

CONFLICT OF INTEREST

The authors report no conflicts of interest.

REFERENCES

[1]Aguado, A. M., A. L. Olivares, C. Yagüe, E. Silva, M. Nuñez-García, A. Fernandez-Quilez, J. Mill, I. Genua, D. Arzamendi, T. De Potter, X. Freixa, and O. Camara. In silico optimization of left atrial appendage occluder implantation using interactive and modeling tools. *Front. Physiol.* 10:237, 2019.

[2]Al-Saady, N. M., O. A. Obel, and A. J. Camm. Left atrial appendage: structure, function, and role in thromboembolism. *Heart* 82:547–554, 1999.

[3]Bai, W., Z. Chen, H. Tang, H. Wang, W. Cheng, and L. Rao. Assessment of the left atrial appendage structure and morphology: comparison of real-time three-dimensional transesophageal echocardiography and computed tomography. *Int. J. Cardiovasc. Imaging* 33:623–633, 2017.

[4]Bermejo, J., P. Martıńez-Legazpi, and J. C. del AĺAmo. The clinical assessment of intraventricular flows. *Annu. Rev. Fluid Mech.* 47:315–342, 2015.

[5]Biase, L. D., A. Natale, and J. Romero. Thrombogenic and arrhythmogenic roles of the left atrial appendage in atrial fibrillation clinical implications. *Circulation* 138:2036–2050, 2018.

[6]Bosi, G. M., A. Cook, R. Rai, L. J. Menezes, S. Schievano, R. Torii, and G. Burriesci. Computational fluid dynamic analysis of the left atrial appendage to predict thrombosis risk. *Front. Cardiovasc. Med.* 5:1–8, 2018.

[7]Buchmann, N. A., C. Atkinson, M. C. Jeremy, and J. Soria. Tomographic particle image velocimetry investigation of the flow in a modeled human carotid artery bifurcation. *Exp. Fluids* 50:1131–1151, 2011.

[8]Cha, Y.-M., M. M. Redfield, W.-K. Shen, and B. J. Gersh. Atrial fibrillation and ventricular dysfunction: a vicious electromechanical cycle. *Circulation* 109:2839–2843, 2004.

[9]Chanda, A. and J. P. Reilly. Left atrial appendage occlusion for stroke prevention. *Prog. Cardiovasc. Dis.* 59:626–635, 2017.

[10]Charonko, J. J., P. P. Vlachos. Estimation of uncertainty bounds for individual particle image velocimetry measurements from cross-correlation peak ratio. *Meas. Sci. Technol.* 24, 2013.

[11]Chnafa, C., S. Mendez, and F. Nicoud. Image-based large-eddy simulation in a realistic left heart. *Comput. Fluids* 94:173–187, 2014.

[12]Christiaens, L., N. Varroud-Vial, P. Ardilouze, S. Ragot, J. Mergy, B. Bonnet, D. Herpin, and J. Allal. Real three-dimensional assessment of left atrial and left atrial appendage volumes by 64-slice spiral computed tomography in individuals with or without cardiovascular disease. *Int. J. Cardiol.* 140:189–196, 2010.

[13]Dahl, S. K., E. Thomassen, L. R. Hellevik, and B. Skallerud. Impact of Pulmonary Venous Locations on the Intra-Atrial Flow and the Mitral Valve Plane Velocity Profile. *Cardiovasc. Eng. Technol.* 3:269–281, 2012.

[14]Di Biase, L., P. Santangeli, M. Anselmino, P. Mohanty, I. Salvetti, S. Gili, R. Horton, J. E. Sanchez, R. Bai, S. Mohanty, A. Pump, M. CerecedaBrantes, G. J. Gallinghouse, J. D. Burkhardt, F. Cesarani, M. Scaglione, A. Natale, and F. Gaita. Does the left atrial appendage morphology correlate with the risk of stroke in patients with atrial fibrillation? Results from a multicenter study. *J. Am. Coll. Cardiol.* 60:531–538, 2012.

[15]Fyrenius, A., L. Wigstro̊m̃, T. Ebbers, M. Karlsson, J. Engvall, and A. F. Bolger. Three dimensional flow in the human left atrium. *Heart* 86:448–455, 2001.

[16]Garcıá-Isla, G., A. L. Olivares, E. Silva, M. Nun˜ ez-Garcia, C. Butakoff, D. Sanchez-Quintana, H. G. Morales, X. Freixa, J. Noailly, T. De Potter, and O. Camara. Sensitivity analysis of geometrical parameters to study haemodynamics and thrombus formation in the left atrial appendage. *Int. J. Numer. Methods Biomed. Eng.* 34:e3100, 2018.

[17]Go, A. S., E. M. Hylek, K. A. Phillips, Y. Chang, L. E. Henault, J. V. Selby, and D. E. Singer. Prevalence of diagnosed atrial fibrillation in adults: national implications for rhythm management and stroke prevention: the anticoagulation and risk factors in atrial fibrillation study. *JAMA* 285:2370–2375, 2001.

[18]Holmes, D. R., D. R. Lakkireddy, R. P. Whitlock, R. Waksman, and M. J. Mack. Left atrial appendage occlusion: opportunities and challenges. *J. Am. Coll. Cardiol.* 63:291–298, 2014.

[19]Lantz, J., V. Gupta, L. Henriksson, M. Karlsson, A. Persson, C. J. Carlhaĺl, and T. Ebbers. Impact of pulmonary venous inflow on cardiac flow simulations: comparison with in vivo 4D Flow MRI. *Ann. Biomed. Eng.* 47:413–424, 2019.

[20]Lip, G. Y., N. Al-Saady, J. Jin, M. Sun, M. Melino, S. M. Winters, D. Zamoryakhin, and A. Goette. Anticoagulation control in warfarin-treated patients undergoing cardioversion of atrial fibrillation (from the edoxaban versus enoxaparin-warfarin in patients undergoing cardioversion of atrial fibrillation trial). *Am. J. Cardiol.* 120:792–796, 2017.

[21]Loudon, C. and A. Tordesillas. The use of the dimensionless Womersley number to characterize the unsteady nature of internal flow. *J. Theor. Biol.* 191:63–78, 1998.

[22]Lupercio, F., J. CarlosRuiz, D. F. Briceno, J. Romero, P. A. Villablanca, C. Berardi, R. Faillace, A. Krumerman, J. D. Fisher, K. Ferrick, M. Garcia, A. Natale, and L. Di Biase. Left atrial appendage morphology assessment for risk stratification of embolic stroke in patients with atrial fibrillation: a meta-analysis. *Heart Rhythm* 13:1402–1409, 2016.

[23]Masci, A., L. Barone, L. Dede` , M. Fedele, C. Tomasi, A. Quarteroni, and C. Corsi. The impact of left atrium appendage morphology on stroke risk assessment in atrial fibrillation: a computational fluid dynamics study. *Front. Physiol.* 9:1–11, 2019.

[24]Otani, T., A. Al-Issa, A. Pourmorteza, E. R. McVeigh, S. Wada, and H. Ashikaga. A computational framework for personalized blood flow analysis in the human left atrium. *Ann. Biomed. Eng.* 44:3284–3294, 2016.

[25]Pellman, J. and F. Sheikh. Atrial fibrillation: mechanisms, therapeutics, and future directions. *Compr. Physiol.* 5:649–665, 2015.

[26]Singh, S. M., A. Micieli, and H. C. Wijeysundera. Economic evaluation of percutaneous left atrial appendage occlusion, dabigatran, and warfarin for stroke prevention in patients with nonvalvular atrial fibrillation. *Circulation* 127:2414–2423, 2013.

[27]Vedula, V., R. George, L. Younes, and R. Mittal. Hemodynamics in the left atrium and its effect on ventricular flow patterns. *J. Biomech. Eng.* 137:1–8, 2015.

[28]Willert, C. E. and M. Gharib. Digital particle image velocimetry. *Exp. Fluids* 10:181–193, 1991.

[29]Zhong, L., J. M. Zhang, B. Su, R. S. Tan, J. C. Allen, and G. S. Kassab. Application of patient-specific computational fluid dynamics in coronary and intra-cardiac flow simulations: challenges and opportunities. *Front. Physiol.* 9:742, 2018.